Potential Formation Triggered by Field-Aligned Electron Acceleration Due to Electron Cyclotron Resonance along Diverging Magnetic-Field Lines

Toshiro Kaneko, Rikizo Hatakeyama, and Noriyoshi Sato

***Abstract*—Stationary potential drop and ion acceleration along diverging magnetic-field lines are observed in a fully ionized collisionless plasma flow in the presence of electron cyclotron resonance (ECR) heating (ECRH). Time-resolved measurements for the purpose of clarifying the potential-formation dynamics show that temporal evolutions of the potential profile and electron energy distribution function correlate well with each other. The strong potential drop is found to be caused by a field-aligned electron acceleration due to ECRH, being accompanied by an effective ion acceleration so as to maintain the charge neutrality condition in the downstream region from the ECR point.**

***Index Terms*—Diverging magnetic-field lines, electron cyclotron resonance, ion acceleration, stationary potential drop.**

I. Introduction

CHARGED particles in a plasma flow along diverging magnetic-field lines basically undergo acceleration by a magnetic force $-\mu\nabla_{||}B$, where μ and $\nabla_{||}B$ are magnetic moment and field gradient parallel to magnetic field lines, respectively. In general, the charged-particle magnetic moment can easily be increased because there exist various kinds of heating mechanisms in magnetized plasmas. This simple acceleration by $-\mu\nabla_{||}B$ force has been recognized to be an important process in conjunction with ion conic formation in the ionosphere, which is considered to be due to perpendicular heating and adiabatic upwelling of the ions along auroral field lines [1]–[4]. When electron heating perpendicular to magnetic field lines preferentially occurs in a gradient region of magnetic field, on the other hand, the resultant force of $-\mu\nabla_{||}B$ is expected to induce charge separation, leading to plasma potential formation along inhomogeneous magnetic-field lines [5], [6]. In relation to this viewpoint, measurements along open magnetic-field lines in end regions of tandem mirror devices [7], [8] have been made for overall understanding of the potential formation which is the key point for fusion plasma confinement. In basic laboratory experiments, an effect of diverging magnetic-field gradient on anode double layers is investigated [9]. To our knowledge, however, no clear-cut experimental result has been reported on a relation between $-\mu\nabla_{||}B$ charged-particle acceleration and the potential formation in diverging magnetic-field lines. Here, our concern is to clarify details of the potential formation triggered by field-aligned electron acceleration of $-\mu\nabla_{||}B$ due to electron cyclotron resonance (ECR) heating (ECRH).

Since the potential structure formed is considered to be accompanied by ion acceleration, furthermore, our approach plays a crucial role in discussing details of the mechanism of the solar wind expansion [10], plasma thrust by expansion in a magnetic nozzle [11], ion impinging in reactive plasma processing [12]–[14], and ion beam generation for material processing. In particular, behaviors of ion beam generated by using space charge rather than grids have not been clarified in detail, which are important for a high-rate and high-quality material processing. Thus, it is also indispensable to clarify a relation between the potential structure and resultant ion acceleration.

In this paper, temporally and spatially detailed measurements are performed on not only potential formation but also particle acceleration in the presence of the single ECR point located in a gradient region of a simple diverging magnetic field. A brief result of this work has been reported earlier [15]. In Section II, an experimental apparatus and methods are described. Experimental results are presented in Section III and are discussed in Section IV. Conclusions are included in Section V.

II. Experimental Apparatus

The experiment is performed with a fully-ionized plasma which is produced by surface ionization of potassium atoms on a 6.0-cm-diameter hot tungsten plate at one end ($z = +160$ cm) of a single-ended Q machine [16], [17] under an electron-rich condition, as shown schematically in Fig. 1. Ions are accelerated by a potential drop of the electron sheath just in front of the hot plate which is grounded electrically, together with a 20.8-cm-diameter vacuum chamber. Initial ion flow energy E_{i0} depends on the sheath potential which can be varied by changing the hot-plate power and/or influx quantity of potassium atoms. There is a tungsten grid (0.03-mm-diameter wire, 50 mesh/in) at a distance of 40 cm from the hot plate, which is used as a gate to inject a plasma flow. To the grid which is biased negatively with respect to the hot plate, a step potential ϕ_g up to the plasma potential is applied in order to inject the plasma flow along the magnetic field [18].

A small movable Langmuir probe is used to measure plasma parameters including an electron energy distribution function $F_e(V_c)$ and their axial profiles. An ion energy distribution function parallel to the magnetic field $F_{i||}(V_c)$ is measured by a directional electrostatic energy analyzer. $F_e(V_c)$ and $F_{i||}(V_c)$ are

Manuscript received March 22, 2000; revised June 1, 2000.

The authors are with the Department of Electrical Engineering, Tohoku University, Sendai 980-8577, Japan (e-mail: kaneko@ecei.tohoku.ac.jp).

Publisher Item Identifier S 0093-3813(00)09975-6.

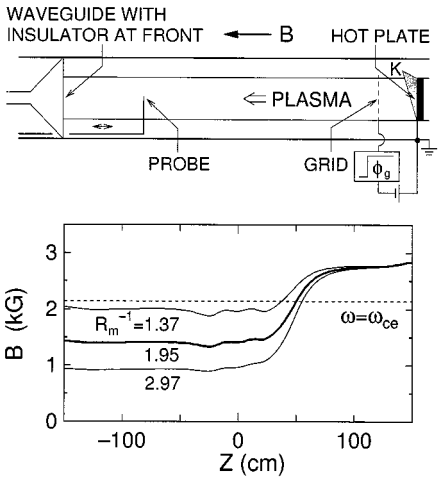

Fig. 1. Schematic of experimental apparatus and diverging magnetic-field configuration.

obtained from the first derivatives dI_c/dV_c [19], where I_c is the current flowing to the probe or a collector of the energy analyzer, and V_c is the voltage of the probe or the collector applied with respect to the hot plate. Here, V_c yielding the peak of $F_e(V_c)$ determines the plasma potential. In our typical case, the plasma density n_{p0} is around 1×10^9 cm^{-3}, the electron temperature T_{e0} is approximately 0.2 eV, the ion temperature $T_{i0} \lesssim T_{e0}$, and the initial ion flow energy $E_{i0} \simeq 1 \sim 2$ eV. A background gas pressure is 5×10^{-5} Pa. Under such a condition, the collision mean free paths of electrons and ions are longer than the plasma length and, from this point of view, the plasma is collisionless. Typical diverging magnetic-field configurations are shown at the bottom of Fig. 1. The magnetic field has a 50-cm-length gradient region sandwiched between a 80-cm-length and a 170-cm-length relatively flat regions. The magnetic field is changed so as to vary the degree of field divergence R_m^{-1} (reciprocal of so-called mirror ratio R_m) in the range of $1 \sim 3$, which is defined as ratio of the magnetic-field strength in the strong region to that in the weak region.

A microwave with frequency $\omega/2\pi = 6$ GHz and input power $P_\mu = 0 \sim 1$ W is launched into the plasma through a circular waveguide located on the opposite side of the hot plate. A waveguide window is covered with an insulator which terminates the plasma column at $z = -150$ cm as an end plate. The microwave propagates toward an ECR point ($\omega = \omega_{ce}$) from the weak to the strong magnetic-field strength regions, where $\omega_{ce}/2\pi$ is the electron cyclotron frequency. In this situation, the wave approaches the ECR point from its cutoff-point side, and the wave amplitude might decrease in the evanescent region. In our experimental condition of low n_{p0}, however, the evanescent region is very narrow ($\simeq$0.1 cm) in comparison with the wave length ($\simeq$5 cm) because of the condition $\omega_{pe} \ll \omega_{ce}$, where $\omega_{pe}/2\pi$ is the electron plasma frequency. Thus, the wave passes through the evanescent region by a tunneling effect [20], [21] and ECR can take place beyond the cut-off point. A subscript "0" stands for the parameters without microwave injection. To clarify dynamics of the plasma particles accompanied by the potential formation, we measure spatial and temporal evolutions of the plasma parameters. Here, time-resolved measurements are performed by a usual boxcar sampling technique with time resolution of about 1 μs, where probe-current pulses are averaged in a synchronous detection mode.

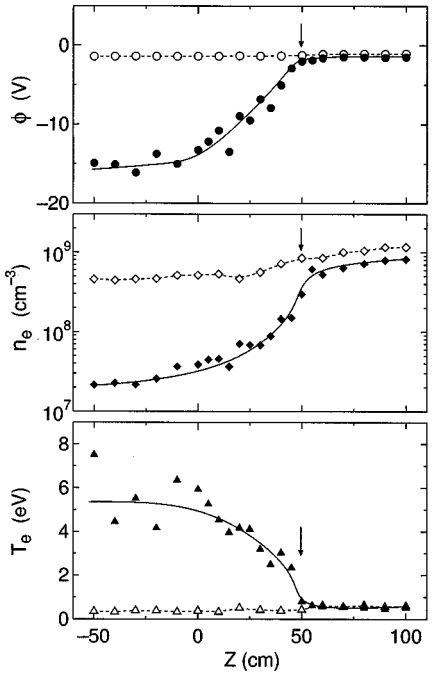

Fig. 2. Spatial profiles of plasma potential ϕ, electron density n_e, and electron temperature T_e in the steady state with $R_m^{-1} = 1.95$ for $P_\mu = 0$ W (open marks) and 0.5 W (closed marks).

III. Experimental Results

A. Potential Formation

Measurements of axial profiles of plasma potential ϕ, electron density n_e, and electron temperature T_e at the radial center are performed in the steady state with $R_m^{-1} = 1.95$ for $P_\mu = 0$ W (open marks) and $P_\mu = 0.5$ W (closed marks), as shown in Fig. 2. Here, T_e measured by our Langmuir probe gives the average value of the electron temperatures parallel and perpendicular to the magnetic field lines, and arrows at $z = 50$ cm indicate the position of ECR point. ϕ is almost constant spatially in the upstream region for both $P_\mu = 0$ W and 0.5 W. In the downstream region from the ECR point, on the other hand, ϕ strongly decreases along the plasma flow for $P_\mu = 0.5$ W. This profile is similar to that of the magnetic-field strength. The absolute value of this potential drop $|\Delta\phi|$, which is the potential difference between the upstream ($z = 100$ cm) and downstream ($z = -100$ cm) regions, is more than 15 V. The potential drop $\Delta\phi$ is expected to lead to the acceleration of ions toward the downstream region as will also be described later. n_e decreases along the magnetic-field lines even for $P_\mu = 0$ W, and n_e in the downstream region becomes 40% of that in the upstream region. This is because the cross section of plasma column in the downstream region becomes about twice that in the upstream region in the case of $R_m^{-1} \simeq 2$ and the amount of electron acceleration parallel to the magnetic field attains to 1.2 times by transferring the perpendicular energy of the isotropic electrons to the parallel energy. For $P_\mu = 0.5$ W, on the other hand, n_e

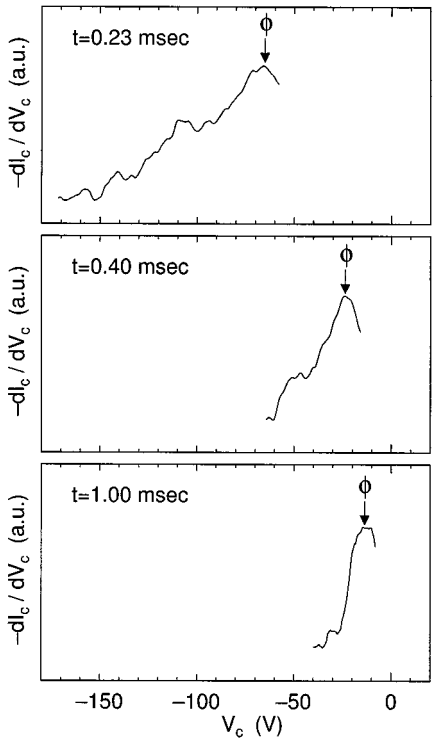

Fig. 3. Temporal evolution of the electron energy distribution $F_e(V_c)$ with $R_m^{-1} = 1.95$ for $P_\mu = 0.5$ W at $z = -100$ cm.

drastically decreases beyond the ECR point, where n_e is smaller than n_{e0} by an order of magnitude. This decrease in n_e will be discussed in Section IV in connection with the drop of ϕ. T_e in the downstream region from the ECR point increases along the magnetic field lines for $P_\mu = 0.5$W. $T_e \simeq 5$ eV is attained at $z = -50$ cm, which is caused by the heating due to ECR and the conversion of the perpendicular energy into the parallel energy.

In order to clarify dynamics of the potential formation, temporal evolutions of an energy distribution of electrons $F_e(V_c)$ after injection of the plasma flow at $t = 0$ ms (rising phase of ϕ_g) are measured at $z = -100$ cm in the case of $R_m^{-1} = 1.95$ and $P_\mu = 0.5$ W, as shown in Fig. 3. Concerning the interpretation of $F_e(V_c)$, we apply average electron energy E_e instead of the electron temperature T_e, which is obtained from the slope of the semi-log plots of the I_c–V_c characteristics in the bulk and tail region of the electron distribution, because the electron energy distribution is not thermalized in this time scale after perpendicular heating by ECR and energy transformation through $-\mu\nabla_{\|}B$ force. Thus, E_e and T_e are used in the temporal and steady state cases, respectively. At the time $t = 0.23$ ms, V_c yielding the peak of $F_e(V_c)$ attains to -66 V, which is marked by an arrow and denotes the plasma potential. Thus, the potential drop $|\Delta\phi|$ transiently increases by several times that in the steady state. Furthermore, the average electron energy E_e at $t = 0.23$ ms increases over 30 eV which is more than six times higher than T_e in the steady state. Both $|\Delta\phi|$ and E_e gradually decrease as time goes by and $F_e(V_c)$ at $t = 1.0$ ms is almost the same as in the steady state. More detailed time-resolved measurements of a) the average electron energy E_e and b) the plasma potential ϕ are performed for $P_\mu = 0.5$ W at $z = 100$ cm (open marks) and $z = -100$ cm (closed marks), as shown in

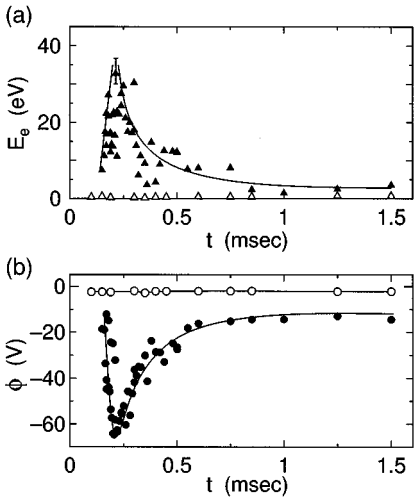

Fig. 4. (a) Average electron energy E_e and (b) plasma potential ϕ as a function of time with $R_m^{-1} = 1.95$ for $P_\mu = 0.5$ W. Open and closed marks denote $z = 100$ cm and $z = -100$ cm, respectively.

Fig. 4. When a front of the plasma-flow pulse arrives around the ECR point ($t = 0.15$ ms), E_e in the region downstream from the ECR point ($z = -100$ cm) is measured to be extremely high up to $E_e/T_{e0} > 10^2$, which is due to proceeding electrons heated by ECR, while almost no change of E_e is observed in the upstream region ($z = 100$ cm). In this case, ϕ in the downstream region is measured to become extremely negative while there is no change of ϕ in the upstream region, where the spatial difference between them attains to $|\Delta\phi| \gtrsim 60$ V. As the bulk plasma continuously passes through the ECR point ($t \gtrsim 0.23$ ms), E_e and $|\Delta\phi|$ gradually decrease, approaching a steady state ($|\Delta\phi| \simeq 15$ V, $T_e \simeq 5$ eV). It can be seen from this figure that the decrease and the increase in ϕ correspond to the increase and the decrease in E_e, respectively.

Fig. 5 presents a temporal evolution of axial ϕ profile for $P_\mu = 0.5$ W. A kind of ambipolar potential with a large potential difference ($e|\Delta\phi|/T_{e0} > 10^2$) is observed to extend over a long distance toward the region downstream from the ECR point when the ECR of front electrons in the expanding plasma is initiated ($t \simeq 0.15$ ms). After the front electrons reach the end-plate and begin to be reflected by an ion sheath in front of the end-plate ($t \gtrsim 0.2$ ms), the potential gradient is found to be localized ahead of the ECR point. This phenomenon is considered to be caused by the effect that the electrons are reflected and trapped between the end-plate and the magnetic gradient region. The potential drop $\Delta\phi$ is gradually filled up after the arrival of the bulk electrons and ions at the ECR point ($t > 0.23$ ms), and the steady state potential structure is finally formed ($t \gtrsim 1$ ms).

The potential structures in the steady state are presented with P_μ as a parameter in Fig. 6, where $R_m^{-1} = 1.95$. For $P_\mu = 0$ W, a slight potential drop ($\simeq -T_{e0}/e$) is recognized in the downstream region beyond the magnetic gradient. In the case of $P_\mu \neq 0$ W, however, ϕ evidently decreases along magnetic field lines even for $P_\mu = 0.1$ W. $|\Delta\phi|$ increases with an increase in P_μ, attaining to about 20 V for $P_\mu = 1.0$ W. In all the cases of P_μ, ϕ begins to drop at the same axial position, which corresponds to the ECR point indicated by an arrow. In Fig. 7(a), $|\Delta\phi|$ and T_e in the steady state are plotted

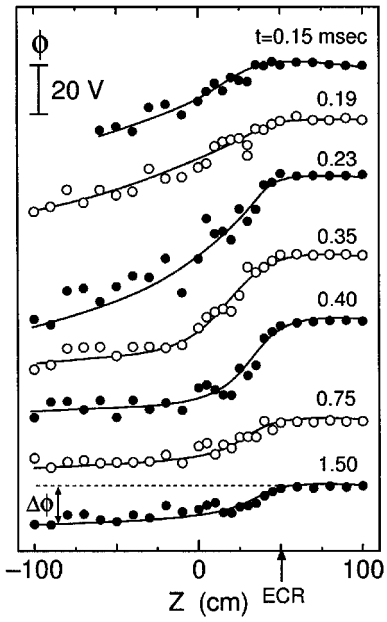

Fig. 5. Temporal evolutions of axial plasma potential profile ϕ after the plasma flow is injected at $t = 0$ ms with $R_m^{-1} = 1.95$ for $P_\mu = 0.5$ W.

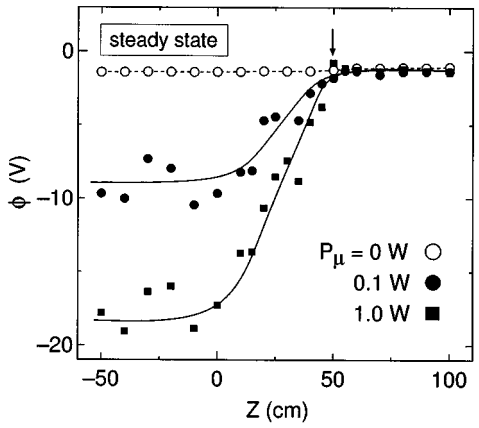

Fig. 6. Spatial profiles of plasma potential ϕ in the steady state with P_μ as a parameter in the case of $R_m^{-1} = 1.95$

as a function of P_μ with $R_m^{-1} = 1.95$. $|\Delta\phi|$ increases with an increase in P_μ, followed by a gradual saturation. In this case, T_e increases in a quite similar way to $|\Delta\phi|$, where T_e is the spatially averaged value in the downstream region of $z = -100 \sim -30$ cm. $|\Delta\phi|$ and E_e at the time $t = 0.23$ ms, when $|\Delta\phi|$ has the maximum value, are plotted as a function of P_μ in Fig. 7(b), where E_e is also the spatially averaged value the same as T_e. Although $|\Delta\phi|$ at $t = 0.23$ ms is about four times larger than that in the steady state for any P_μ, the properties of dependence on P_μ are the same each other. Added to this, E_e also increases in a quite similar way to $|\Delta\phi|$ at $t = 0.23$ ms. These results indicate that $|\Delta\phi|$ is closely related to E_e and T_e, which is discussed in Section IV.

In Fig. 8, spatial profiles of ϕ in the steady state are plotted with R_m^{-1} as a parameter for $P_\mu = 0.5$ W. With an increase in R_m^{-1}, ϕ in the downstream region more deeply drops. The axial position at which ϕ begins to drop shifts toward the positive direction of z when R_m^{-1} is increased, because the axial position

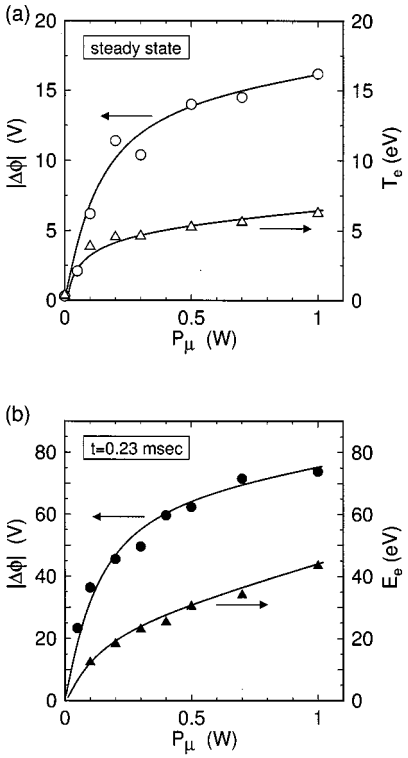

Fig. 7. (a) Potential differences $|\Delta\phi|$ (open circles) and electron temperature T_e (open triangles) in the steady state and (b) $|\Delta\phi|$ (closed circles) and electron energy E_e (closed triangles) at $t = 0.23$ ms in the downstream region of $z = -100 \sim -30$ cm as a function of P_μ with $R_m^{-1} = 1.95$.

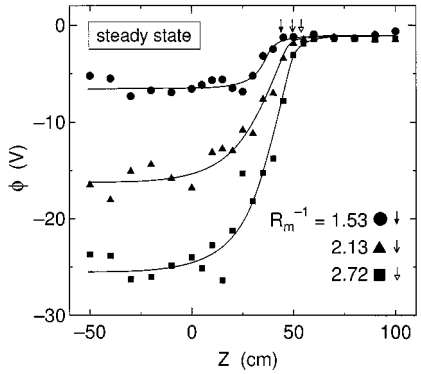

Fig. 8. Spatial profiles of plasma potential ϕ in the steady state with R_m^{-1} as a parameter for $P_\mu = 0.5$ W.

of the ECR point correspondingly moves to the right with the change in R_m^{-1} as indicated by three different types of arrows. Dependences of $|\Delta\phi|$ on R_m^{-1} at $t = 0.23$ ms and in the steady state for $P_\mu = 0.5$ W are presented in Fig. 9. The potential drops are linearly enhanced with an increase in R_m^{-1} and do not show a tendency to be saturated. For $R_m^{-1} \lesssim 1.3$, the potential difference is too small to be detected because the magnetic-field strength in the downstream region (weak field region) is larger than that corresponding to ECR ($B = 2.14$ kG) and the ECR point exists nowhere.

B. Ion Acceleration

The potential structure observed so far is considered to have the function to accelerate the ions toward the downstream region

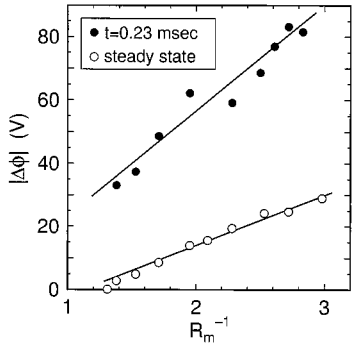

Fig. 9. Potential differences $|\Delta\phi|$ as a function of R_m^{-1} for $P_\mu = 0.5$ W. Closed and open marks denote values at $t = 0.23$ ms and in the steady state, respectively.

by the potential gradient. In order to investigate the detailed situation of the ion acceleration, an ion energy distribution function parallel to the magnetic field $F_{i\|}(V_c)$ is measured. The electron energy distribution function $F_e(V_c)$ is also measured for the comparison with $F_{i\|}(V_c)$.

Axial variations of $F_e(V_c)$ and $F_{i\|}(V_c)$ in the steady state with $R_m^{-1} = 1.95$ for $P_\mu = 0$ W (dotted lines) and $P_\mu = 0.5$ W (solid lines) are typically shown in Fig. 10, where all the peak heights are adjusted to the same value because our attention is focused on V_c yielding the peaks. Fig. 10(a) shows $F_e(V_c)$ and $F_{i\|}(V_c)$ in the upstream region ($z = 100$ cm). No appreciable difference of $F_e(V_c)$ and $F_{i\|}(V_c)$ is found between the cases of $P_\mu = 0$ W and 0.5 W, although the electron and ion temperatures slightly change. Here, V_c yielding the peak of $F_e(V_c)$ indicates the plasma potential $\phi(\simeq -1.5$ V), which coincides with the result in Fig. 2. V_c yielding the peak of $F_{i\|}(V_c)$ shifts from that of $F_e(V_c)$ toward the positive value of V_c by about 1.5 V. This difference of V_c shows that the initial ion flow energy $E_{i0} \simeq 1.5$ eV is generated by the electron sheath in front of the hot plate. Fig. 10(b) shows $F_e(V_c)$ and $F_{i\|}(V_c)$ in the downstream region ($z = -35$ cm). For $P_\mu = 0$ W, $F_e(V_c)$ and $F_{i\|}(V_c)$ are almost the same as in the upstream region, but the parallel ion flow energy E_i, which is defined as the V_c difference between the peaks of $F_e(V_c)$ and $F_{i\|}(V_c)$ at each position of z, becomes slightly smaller with distance. This decrease in E_i is considered to be caused by some kinds of energy dissipations of the ion flow. For $P_\mu = 0.5$ W, on the other hand, $F_e(V_c)$ in the downstream region is measured to greatly shift to the negative value of V_c and to consist of electrons with a higher temperature of $T_e \simeq 5$ eV. This peak shift corresponds to the plasma potential drop $|\Delta\phi| \simeq 15$ V in Fig. 2. Since V_c yielding the peak of $F_{i\|}(V_c)$ almost never changes even in the downstream region, i.e., it relatively shifts from the plasma potential [the peak of $F_e(V_c)$] toward the largely positive value of V_c, the ions turn out to have a directional energy parallel to the magnetic field, forming the ion beam flowing downstream. The ion flow energy E_i is found to be nearly equal to the value equivalent of $|\Delta\phi|$. Judging from the above, the ion acceleration is closely related to the potential formation.

According to measurements of the parallel ion flow energy E_i (closed diamond) in the steady state with R_m^{-1} as a parameter for $P_\mu = 0.5$ W at $z = -35$ cm, it is found that ions are greatly accelerated along the field lines to attain to E_i corresponding to

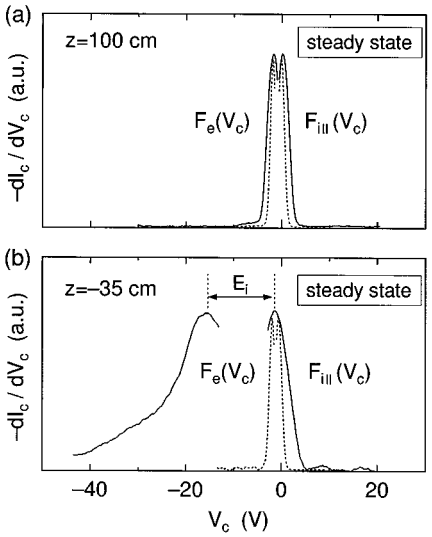

Fig. 10. Energy distributions of electrons $F_e(V_c)$ and ions parallel to the magnetic field $F_{i\|}(V_c)$ in the steady state with $R_m^{-1} = 1.95$ for $P_\mu = 0$ W (dotted lines) and $P_\mu = 0.5$ W (solid lines). (a) At $z = 100$ cm. (b) At $z = -35$ cm.

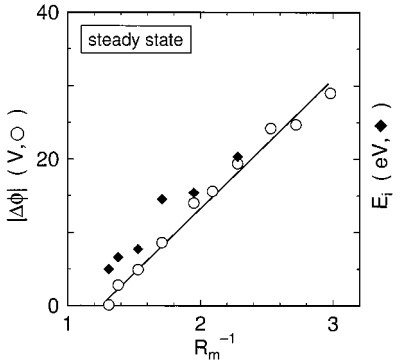

Fig. 11. Potential differences $|\Delta\phi|$ (open circles) and parallel ion energy E_i (closed diamonds) at $z = -35$ cm as a function of R_m^{-1} for $P_\mu = 0.5$ W in the steady state.

$e|\Delta\phi|$ (open circles), as shown in Fig. 11. In this figure, E_i is observed to be larger than $e|\Delta\phi|$ by a few electron Volts, which can be explained by adding the initial ion flow energy $E_{i0} \simeq 1.5$ eV to the value equivalent of potential drop $e|\Delta\phi|$.

In order to investigate the correlation between the large potential drop formed transiently at the front of the plasma flow (see Fig. 5) and the transient ion acceleration, temporal evolutions of ion saturation current J_{is} of the probe are shown as a function of the axial distance z in Fig. 12, where $R_m^{-1} = 1.95$, $P_\mu = 0.5$ W. Here, a dotted line indicates the time at which preceding ions get to each position of z. For $P_\mu = 0$ W, ions are observed to expand at a constant speed of 5×10^5 cm/s, which is the value equivalent to the flow energy of about 5 eV. This flow energy is larger than the initial flow energy E_{i0} ($\simeq$1.5 eV) described above, because it indicates the speed of the preceding ions consisting of a tail component of the ion velocity distribution function while E_{i0} measured by the energy analyzer indicates the speed of the bulk-component ions. For $P_\mu = 0.5$ W, on the other hand, the ions are observed to get to each position of z faster than the case of $P_\mu = 0$ W. This result shows that the ions are accelerated by the electrostatic potential formed in the downstream region. The

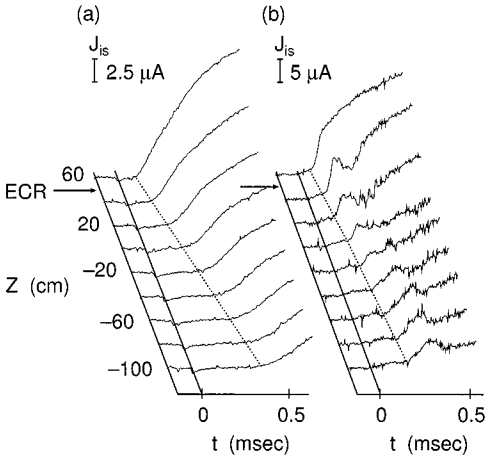

Fig. 12. Temporal evolutions of ion saturation current J_{is} profile along the plasma column with $R_m^{-1} = 1.95$. (a) For $P_\mu = 0$ W. (b) For $P_\mu = 0.5$ W.

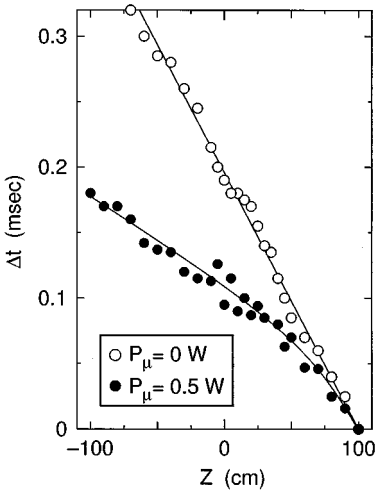

Fig. 13. Time delay Δt of a front of the expanding ion flow along the plasma column after the preceding ions pass through the position at $z = 100$ cm with $R_m^{-1} = 1.95$ for $P_\mu = 0$ W (open marks) and $P_\mu = 0.5$ W (closed marks).

situation of the ion acceleration is more clearly demonstrated in Fig. 13, which presents time delays Δt at each position of z after the preceding ions pass through the position at $z = 100$ cm in the cases of $P_\mu = 0$ W (open circles) and 0.5 W (closed circles). The ions are found to be strongly accelerated in the downstream region from the ECR point ($z = 50$ cm) in the presence of ECRH. This acceleration of the ions is ended at $z \simeq 0$ cm. Thereafter, the ions are expanding with the constant velocity. Here, the expanding speed of the ions in the downstream region are calculated to be 1.4×10^6 cm/s, which is the value equivalent to the flow energy of about 40 eV.

IV. Discussions

Let us mention the mechanism of the potential formation. As described above, the large potential drop is observed in the region downstream from the ECR point under the diverging-field configuration. At the ECR point, the electrons are accelerated by the ECR in the direction perpendicular to the magnetic field and are accelerated in the axial direction by $-\mu\nabla_{||}B$ force along the magnetic-field lines. n_e in the downstream region drastically decreases as shown in Fig. 2 because of the conservation of the electron flux, while ions are not directly affected by the ECR. Thus, the strong ambipolar potential leading to the ion acceleration is considered to be formed so as to maintain the charge neutrality condition in the region downstream from the ECR point. In the steady state, the value of the potential drop $|\Delta\phi|$ is about 15 V for $P_\mu = 0.5$ W with $R_m^{-1} = 1.95$, where the electron temperature T_e in the downstream region is about 5 eV, as shown in Fig. 2. This T_e in the downstream region is ten times higher than that in the upstream region ($\simeq 0.5$ eV), as also seen in Figs. 2 and 10. In order to maintain the charge neutrality condition in the downstream region, ions must be accelerated in the same rate as electrons. Because the initial ion flow energy E_{i0} in the upstream region is about 1.5 eV as described above, the ion flow energy E_i in the downstream region must reach the value of about 15 eV. Thus, it is considered that the required $|\Delta\phi|$ which accelerates ions should be about 15 V. When P_μ and R_m^{-1} are increased, the electron energy perpendicular to the magnetic field increases and the conversion of the perpendicular energy into the parallel energy is enhanced, respectively. Since these effects cause the increase in the electron energy parallel to the magnetic-field lines, $|\Delta\phi|$, which accelerates the ions along the magnetic field, is self-consistently increased.

This increase in $|\Delta\phi|$ is quantitatively predicted by a simple flow model, or an ambipolar diffusion model. The ambipolar electric field E can be written

$$E = -\nabla\phi = \frac{D_i - D_e}{\mu_i + \mu_e}\frac{\nabla n}{n} \tag{1}$$

where D_i, D_e, and μ_i, μ_e are diffusion coefficients and mobilities of ion and electron, respectively. When we assume $\mu_e \gg \mu_i$ and $D_e \gg D_i$, integration of (1) yields the ambipolar potential difference $\Delta\phi_{am}$

$$\Delta\phi_{am} = \frac{D_e}{\mu_e}\ln\frac{n_d}{n_u} = T_e \ln\frac{n_d}{n_u} \tag{2}$$

where n_d and n_u are electron densities in the downstream and upstream regions, respectively. In Fig. 14, the theoretical values of potential difference $|\Delta\phi_{am}|$ described above are plotted as a function of P_μ, together with experimental results of n_d/n_u (n_d is the spatially averaged value in the region of $z = -100 \sim -30$ cm, and n_u is the value at $z = 55$ cm which is just before the ECR point). Here, $|\Delta\phi_{am}|$ is evaluated by using measured parameters of n_d/n_u in Fig. 14 and $T_e(E_e)$ in Fig. 7. The values of $|\Delta\phi_{am}|$ both in the steady state and at $t = 0.23$ ms are quantitatively in good agreement with the experimental results of $|\Delta\phi|$ in Fig. 7, which means that the estimation of the potential drop using the simple ambipolar diffusion model is valid in our experimental condition. These results show that it is very useful to accelerate ions by the electrostatic potential because the potential difference is easily predicted and controlled by the electron temperature and the density difference. In the case of the increase in P_μ, $|\Delta\phi|$ is gradually saturated, being accompanied by the saturation of T_e or E_e. This saturation of $|\Delta\phi|$ is considered to be caused by the restriction of the increase in T_e or E_e due to some dissipation mechanism.

The ion acceleration can also be recognized in the expansion of the plasma pulse. In Fig. 13, the ion flow energy E_i in the

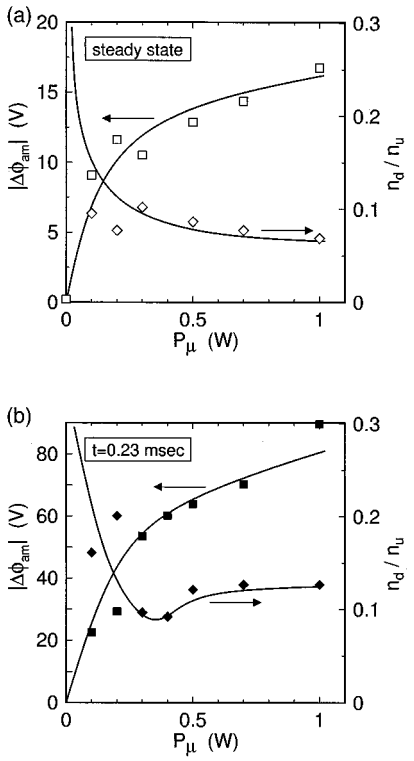

Fig. 14. Theoretical potential differences $|\Delta\phi_{am}|$ (squares) and measured density differences n_d/n_u (diamonds). (a) In the steady state. (b) At $t = 0.23$ ms as a function of P_μ with $R_m^{-1} = 1.95$. $|\Delta\phi_{am}|$ is evaluated by using experimental results of n_d/n_u and $T_e(E_e)$.

presence of ECRH is estimated to be about 40 eV in the downstream region ($z < 0$ cm). This accelerated-ion flow energy is consistent with the observed potential drop $|\Delta\phi|$ of $30 \sim 40$ V at the time of $t = 0.1 \sim 0.2$ ms in Fig. 4. Furthermore, the dependence of E_i on R_m^{-1} is definitely confirmed to be in correspondence with that of $e|\Delta\phi|$, as shown in Fig. 11. It follows from what has been said that the ions are accelerated by the electrostatic potential localized in the magnetic-gradient region due to ECRH and the ion flow energy can be controlled through the self-consistent change of $\Delta\phi$ by externally varying P_μ and/or R_m^{-1}.

V. Conclusion

The strong potential drop $\Delta\phi$ along the diverging magnetic-field lines is observed to be formed in the presence of ECRH in the magnetic gradient region and to be closely related to the electron temperature heated by ECR. It is clarified that the average electron energy and the potential drop transiently increase by several times that in the steady state. This potential formation is triggered by field-aligned electron acceleration leading to effective ion acceleration so as to maintain the charge neutrality condition downstream from the ECR point. The potential-drop value is quantitatively predicted by the ambipolar diffusion model.

It is confirmed that the ions are accelerated by $\Delta\phi$, resulting in attaining to the high flow energy corresponding to $e|\Delta\phi|$. Furthermore, the temporally and spatially detailed measurement of the ion behavior demonstrates that the ion acceleration is localized in the magnetic-gradient region, or the potential-gradient region formed by ECRH. This work could give useful ideas to clarify the mechanism of the ion conic formation, the potential formation in the end region of the tandem mirror, and to control the accelerated-ion energy determined by the potential drop due to local ECR.

Acknowledgment

The authors are indebted to H. Shoji and K. Kojima for their collaborations in the preliminary measurements and H. Ishida for his technical support.

References

[1] G. Lu, P. H. Reiff, T. E. Moore, and R. A. Heelis, "Upflowing ionospheric ions in the auroral region," *J. Geophys. Res.*, vol. 97, pp. 16 855–16 863, 1992.

[2] J. L. Vago, P. M. Kintner, S. W. Chesney, R. L. Arnoldy, K. A. Lynch, T. E. Moore, and C. J. Pollock, "Transverse ion acceleration by localized lower hybrid waves in the topside auroral ionosphere," *J. Geophys. Res.*, vol. 97, pp. 16 935–16 957, 1992.

[3] S. L. Cartier, N. D'Angelo, and R. L. Merlino, "A laboratory study of ion energization by eic waves and subsequent upstreaming along diverging magnetic field lines," *J. Geophys. Res.*, vol. 91, pp. 8025–8033, 1986.

[4] M. Zintl, R. McWilliams, and N. Wolf, "Transverse ion acceleration and ion conic formation in a divergent-field laboratory plasma," *Phys. Plasmas*, vol. 2, pp. 4432–4441, 1995.

[5] R. Geller, N. Hopfgarten, B. Jacquot, and C. Jacquot, "Electric fields parallel to the magnetic field in a laboratory plasma in a magnetic mirror field," *J. Plasma Phys.*, vol. 12, pp. 467–486, 1974.

[6] E. B. Hooper Jr., "Plasma flow resulting from electron cyclotron resonance heating on a magnetic hill," *Phys. Plasmas*, vol. 2, pp. 4563–4569, 1995.

[7] T. Saito, Y. Kiwamoto, K. Kurihara, T. Cho, M. Inutake, S. Miyoshi, T. Tamano, and K. Yatsu, "Scaling study of potential in the end region of a tandem mirror based on end-loss electron measurement," *Phys. Fluids B*, vol. 5, pp. 866–871, 1993.

[8] N. Hershkowitz, B. A. Nelson, J. Johnson, J. R. Ferron, H. Persing, C. Chan, S. N. Golovato, J. D. Callen, and J. Woo, "Enhancement of the plasma potential by fluctuating electric fields near the ion cyclotron frequency," *Phys. Rev. Lett.*, vol. 55, pp. 947–950, 1985.

[9] B. Song, R. L. Merlino, and N. D'Angelo, "The effect of a magnetic field gradient on anode double layers," *Phys. Scripta*, vol. 45, pp. 395–398, 1992.

[10] R. E. Hartle and P. A. Sturrock, "Two-fluid model of the solar wind," *Astrophys. J.*, vol. 151, pp. 1155–1170, 1968.

[11] H. G. Kosmahl, D. B. Miller, and G. W. Bethke, "Plasma acceleration with microwaves near cyclotron resonance," *J. Appl. Phys.*, vol. 38, pp. 4576–4582, 1967.

[12] W. Cronrath, N. Mayumi, M. D. Bowden, K. Uchino, K. Muraoka, and M. Yoshida, "A study of ion velocity distribution functions in processing plasmas produced by electron cyclotron resonance discharges," *J. Appl. Phys.*, vol. 82, pp. 1036–1041, 1997.

[13] Y. Okuno, Y. Ohtsu, and H. Fujita, "Two-dimensional ion velocity distribution functions in electron cyclotron resonance plasma under a divergent magnetic field," *J. Appl. Phys.*, vol. 74, pp. 5990–5996, 1993.

[14] ——, "Effects of downstream magnetic field collimation on ion behavior in electron cyclotron resonance microwave plasma," *IEEE Trans. Plasma Sci.*, vol. 22, pp. 253–259, 1994.

[15] R. Hatakeyama, T. Kaneko, and N. Sato, "Plasma potential formation and particle acceleration due to ecrh in diverging magnetic-field lines," *Trans. Fusion Tech.*, vol. 35, pp. 325–329, 1999.

[16] R. W. Motley, *Q-Machines*. New York: Academic, 1975.

[17] N. Sato, H. Sugai, and R. Hatakeyama, "Spatial evolution of velocity-modulated ion beams in a plasma," *Phys. Rev. Lett.*, vol. 34, pp. 931–934, 1975.

[18] N. Sato, Y. Watanabe, R. Hatakeyama, and T. Mieno, "Potential formation in a high-speed plasma flow along converging magnetic field lines," *Phys. Rev. Lett.*, vol. 61, pp. 1615–1618, 1988.

[19] R. Hatakeyama, N. Sato, Y. Tsunoda, H. Sugai, and Y. Hatta, "Ion-energy distribution in a plasma under a diverging magnetic field," *J. Appl. Phys.*, vol. 45, pp. 85–88, 1974.

[20] D. B. Batchelor, "Budden tunnelling in parallel stratified plasmas," *Plasma Phys.*, vol. 22, pp. 41–55, 1980.
[21] R. F. Ellis, G. D. Tsakiris, and D. A. Boyd, "Emission, absorption, and tunneling of whistler waves in an inhomogeneous magnetic field," *Phys. Fluids*, vol. 26, pp. 1528–1541, 1983.

Toshiro Kaneko was born in Miyagi, Japan, on July 29, 1969. He received the B.E. degree in electronic engineering from Tohoku University, Sendai, Japan, in 1992 and the M.E. and Ph.D. degrees in electronic engineering from Tohoku University in 1994 and 1997, respectively.

He is presently a Research Assistant with the Department of Electrical Engineering, Tohoku University. His research interests are in the fundamental experiments on plasma potential formation and wave propagation related to electron cyclotron resonance.

Rikizo Hatakeyama was born in Akita, Japan, on April 25, 1947. He received the B.E. degree in electronic engineering from Tohoku University, Sendai, Japan, in 1971 and the M.E. and Ph.D. degrees in electronic engineering from Tohoku University in 1973 and 1976, respectively.

He is presently a Professor in the Department of Electronic Engineering, Tohoku University. His research interests are in the fundamental experiments on fullerene plasmas and linear, nonlinear waves in plasmas.

Noriyoshi Sato was born in Miyagi, Japan, on February 4, 1938. He received the B.E. degree in electrical engineering from Tohoku University, Sendai, Japan, in 1960 and the M.E. and Ph.D. degrees in electrical engineering from Tohoku University in 1962 and 1965, respectively.

He is presently a Professor in the Department of Electrical Engineering, Tohoku University. His research interests now are in the fundamental experiments on dusty plasma and nonlinear instabilities and waves in plasmas.